Scripta Materialia 186 (2020) 304–311

Contents lists available at ScienceDirect

Scripta Materialia

journal homepage: www.elsevier.com/locate/scriptamat

Viewpoint set

Towards understanding the structure–property relationships of heterogeneous-structured materials

Jianguo Li[a], Qian Zhang[a], Ruirui Huang[a], Xiaoyan Li[a,*], Huajian Gao[b,c,**]

[a] Center for Advanced Mechanics and Materials, Applied Mechanics Laboratory, Department of Engineering Mechanics, Tsinghua University, Beijing 100084, China

[b] School of Mechanical and Aerospace Engineering, College of Engineering, Nanyang Technological University, 70 Nanyang Drive, Singapore 639798, Singapore

[c] Institute of High Performance Computing, A*STAR, Singapore 138632, Singapore

ARTICLE INFO

Article history:
Received 10 April 2020
Revised 1 May 2020
Accepted 6 May 2020
Available online 5 June 2020

Keywords:
Heterogeneous-structured materials
Structural heterogeneity
Strain gradient plasticity
Geometrically necessary dislocations
Back stress

ABSTRACT

Heterogeneous-structured materials are a new class of metallic materials that have recently emerged due to development of advanced processing and structural/architectural design techniques. These materials are made of heterogeneous domains having different constitutive behaviors and achieve superior mechanical properties, such as extra strengthening and work hardening, that are not accessible to conventional homogeneous-structured materials. Here we review recent experimental, theoretical and computational studies on microstructures, mechanical properties and deformation behaviors of heterogeneous-structured metals/alloys, highlighting the relationships between structural heterogeneity and mechanical property improvements, as well as some perspectives towards achieving fundamental understanding of plastic deformation based on strain gradient theory.

1. Introduction

The strength and work hardening capability of metallic materials can both be enhanced by geometrically necessary dislocations (GNDs) [1,2] that are required to accommodate the lattice curvature arising from inhomogeneous plastic deformation often measured in the form of a plastic strain gradient [3–6]. In addition to GNDs, other dislocations that glide to carry the plastic strain are called statistically stored dislocations (SSDs). The incorporation of GNDs into continuum theories of plasticity has led to the establishment and development of various phenomenological and mechanism-based theories of strain gradient plasticity [3,7–10], where an intrinsic length scale typically on the order of a few microns is often introduced to reflect the effects of strain gradient [3–6]. These theories have been successfully used to explain size-dependent plastic behaviors in metals under different loading conditions [7–10].

In recent years, inspired by biological materials, structural heterogeneity has been applied to engineering metals and alloys through various advanced manufacturing techniques, leading to the emergence of heterogeneous-structured (HS) metallic materials [11–28]. HS metals and alloys are often composed of heterogeneous domains with drastically different constitutive behaviors and mechanical properties. Compared with their homogeneous-structured counterparts, HS metals and alloys have achieved a combination of superior mechanical properties, such as higher strength, better ductility, higher work hardening rate and greater fracture resistance [11–28]. Remarkably, HS metals and alloys can overcome the strength-ductility trade-off, which is a critical deficiency for many homogeneous-structured materials. Experimental studies have indicated that the additional strengthening and hardening of HS metals and alloys can be attributed to inhomogeneous plastic deformation resulting from their intrinsic structural heterogeneity [22–25]. In HS materials with both soft and hard domains, the soft domains usually sustain plastic deformation prior to the hard domain. Compatibility in deformation leads to plastic strain gradients across the domain interfaces, and such strain gradients are accommodated by GNDs [6,22–25]. The GNDs often pile up in the soft domains against their boundaries and act as obstacles that hinder the motion of SSDs, contributing to the work hardening of the material [2,6,22–25,29–38]. Recent experimental and computational studies [14–21] have shown that GNDs indeed play an

* Corresponding author.
** Corresponding author at: School of Mechanical and Aerospace Engineering, College of Engineering, Nanyang Technological University, 70 Nanyang Drive, Singapore 639798, Singapore.
E-mail addresses: xiaoyanlithu@tsinghua.edu.cn (X. Li), huajian.gao@ntu.edu.sg (H. Gao).

https://doi.org/10.1016/j.scriptamat.2020.05.013
1359-6462/

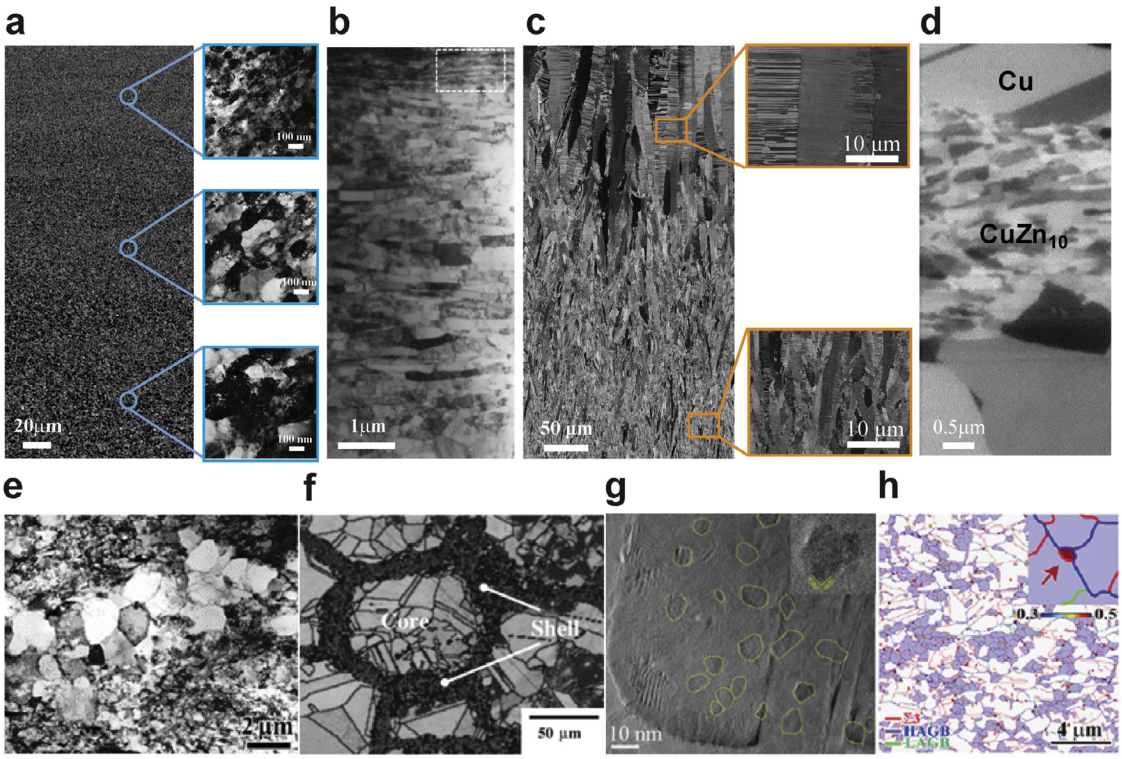

Fig. 1.. Microstructures of various HS metals and alloys. (a) SEM and TEM images of GNG Cu fabricated by surface mechanical rolling treatment [17]. (b) TEM image of GNL Ni produced by surface mechanical grinding treatment [18]. (c) SEM and TEM images of GNT Cu (with a dual gradient in grain size and twin size) fabricated by electrodeposition [20]. (d) SEM image of heterogeneous laminated Cu/$CuZn_{10}$ produced by accumulative roll binding [21]. (e) TEM image of heterogeneous lamella Ti with micrograined lamellae embedded in an ultrafine-grained lamella matrix [16]. (f) EBSD image of bimodal-grained Cu with a harmonic structure [27]. (g) TEM image of nanodomained Ni, where the nanoscale Ni domains with an average size of 7 nm and a small misorientation (<15°) are randomly distributed in the coarse-grained Ni matrix [28]. (h) EBSD image of a CrCoNi alloy with a three-level heterogeneous grain structure, in which the grain size varies from the nanometer to micrometer range. In particular, nanosized grains nucleate at the triple junctions of ultrafine grains [26]. Note that HAGBs and LAGBs represent high-angle and low-angle grain boundaries, respectively.

important role in the plastic deformation of various HS materials resulting in improvement of their mechanical properties. At this point, the structure–property relationships of HS metals and alloys need to be better understood before their potential can be fully explored.

Here, we aim to discuss some recent progresses in understanding the deformation mechanism and structure–property relationships of HS materials from a mechanics point of view. The discussions will cover the microstructural features of various HS metals and alloys fabricated by different processing techniques, highlighting the characteristic length scale of structural heterogeneity. Our attention will then focus on the strengthening and work hardening behaviors of selected HS metallic materials and the underlying deformation mechanisms. Finally, to stimulate more in-depth research on HS materials to optimize their mechanical properties and performance, we conclude with a perspective and outlook on some of the open questions in the field.

2. Microstructures of HS materials

Fig. 1 shows the microstructures of some HS metallic materials recently fabricated by different processing techniques. Materials with structural gradients (such as grain-size gradients, lamella-thickness gradients and twin-size gradients) are typical HS materials. As shown in Fig. 1(a), gradient nanograined (GNG) Cu exhibits an apparent gradient distribution in grain size from the surface layer to inner core. The grain size is approximately 42 nm in the surface layer and then gradually increases to approximately 160–300 nm at depths of 50–100 μm. For a coarse-grained (CG) sample subjected to surface mechanical rolling treatment, this GNG structure is generated on the surface layer with a depth of ~700 μm [17]. Fig. 1(b) shows transmission electron microscopy (TEM) images of gradient nanolaminated (GNL) Ni fabricated by surface mechanical grinding treatment [18]. The topmost layer of such a sample has an average lamella thickness of approximately 20 nm, which is several times smaller than that of the ultrafine structures in Ni induced by conventional severe plastic deformation [18]. Over a depth range from 5 μm to 150 μm, the average thickness gradually increases from ~100 nm to ~390 nm. The gradient structures in GNG and GNL samples are generated from grain refinement under severe plastic deformation, whereas the gradient distribution is mainly determined by the strain rate and strain gradient induced by the surface mechanical treatment [17,18]. Recently, electrodeposition has been used to fabricate gradient nanostructured metallic materials with more precise and controllable gradient distributions [19,20]. Bulk Ni plates with controllable grain-size gradient distributions have been synthesized by continuously adjusting the current density and additive content during electroplating deposition [19]. Mechanical testing on these GNG Ni samples showed that there exists an optimal gradient distribution corresponding to a combination of high strength and good ductility [19]. More recently, gradient nanotwinned (GNT) Cu with gradients in both grain size and twin thickness has been fabricated by stepwise variations in the electrolyte temperature during direct-current electrodeposition. In Fig. 1(c), the average grain size of GNT Cu increases from 2.5 μm to 15.8 μm from bottom to top, and the corresponding average twin thickness increases from 29 nm to 72 nm. Fig. 1(a)–(c) show that in the GNG, GNL and GNT met-

als, the length scale of the gradient nanostructures generally spans from tens to hundreds of micrometers.

Fig. 1(d) shows a scanning electron microscopy (SEM) image of a heterogeneous laminated composite with alternating CG Cu layers and nanostructured $CuZn_{10}$ layers fabricated by accumulative roll bonding [21]. The layer thickness (i.e., interface spacing) is controlled to vary from 3.7 μm to 125 μm. The average grain sizes in the Cu and $CuZn_{10}$ layers are approximately 4.8 μm and 100 nm, respectively. Such a large difference in grain size between neighboring layers produces significant mechanical incompatibility during plastic deformation, which is accommodated by a pileup of GNDs near the interfaces [21]. In situ high-resolution strain mapping near the interfaces indicates that the length scale of the GNDs is approximately 5–6 μm, which is nearly half of the optimal interface spacing corresponding to the best mechanical properties of the heterogeneous laminated composite [21]. In contrast to the samples with gradient and laminated structures, HS metals and alloys with bimodal and multimodal grains have been prepared via thermomechanical routes involving severe plastic deformation followed by appropriate heat treatments [22–25]. Fig. 1(e) and (f) show the microstructures of heterogeneous lamella Ti and bimodal-grained Cu, respectively. The heterogeneous lamella Ti contains micrograined lamellae embedded in an ultrafine-grained lamella matrix [16]. The average grain sizes of micrograined and ultrafine-grained lamellae are approximately 4 μm and 400 nm, respectively. The thickness of micrograined lamellae is up to several to tens of micrometers and reflects the characteristic length scale for the accumulation of GNDs. The heterogeneous lamella Ti is produced by asymmetric rolling and partial recrystallization [16]. The bimodal-grained Cu exhibits a harmonic structure [27], i.e., the soft CG core areas are surrounded by a continuous network of hard ultrafine-grained shell areas. The average grain sizes of CG and ultrafine-grained areas are approximately 28.2 μm and 2.0 μm, respectively. The harmonic structure is produced by mechanical milling followed by spark plasma sintering or hot roll sintering [27]. Experimental studies have shown that bimodal-grained Cu with harmonic structures containing 40% ultrafine grains exhibits the optimum combination of strength and ductility [27]. As a novel class of HS materials, nanodomained Ni has recently been synthesized by pulse electroplating. As shown in Fig. 1(g), such nanodomained Ni contains a large number of nanoscale Ni domains with an average size of 7 nm and small misorientation ($<15°$), which are randomly distributed in the CG Ni matrix [28]. The average spacing between adjacent nanodomains is on the order of tens of nanometers, indicating the presence of abundant domain interfaces. As a result, a high density of GNDs is generated across these interfaces during plastic deformation, leading to self-dispersion strengthening without a second phase [27]. Fig. 1(h) shows an electron backscatter diffraction (EBSD) image of CrCoNi medium-entropy alloy (MEA) with a three-level heterogeneous grain structure. In such heterogeneous MEAs, the grain size spans from hundreds of nanometers to several micrometers. The coarse grains have a mean grain size of 2.3 μm, the intermediate ultrafine grains have a mean grain size ranging from 250 nm to 1 μm, and the smallest nanoscale grains have a grain size of less than 250 nm. These heterogeneous grain structures were fabricated by electromagnetic levitation melting and the following heat treatments. The formation of heterogeneous grain structures is associated with the low stacking fault energy of the alloy. During plastic deformation, many corner twins evolved into nanosized grains at triple junctions of the ultrafine grains [26], which made the grain structure more heterogeneous. This induced a steep strain gradient across neighboring grains, contributing to the high strain hardening and uniform tensile ductility [26].

The HS materials shown in Fig. 1(d)–(h) involve heterogeneous nanostructures with bimodal or multimodal grain sizes that have different spatial arrangements and/or shapes. These heterogeneous nanostructures can play a dual role in dislocation activities, wherein they block and accumulate dislocations while leaving ample space to allow for the multiplication of dislocations [24]. Notably, these HS materials (Fig. 1(d)–(h)) have significant structural heterogeneity and abundant interfaces, which leads to a pronounced strain gradient and associated accumulation of GNDs during deformation, leading to a combination of high strength and good ductility.

3. Strength-ductility synergy and additional work hardening of HS materials

Over the past few years, a number of experimental studies [11–29] have shown that the introduction of various heterogeneous nanostructures into metallic materials is beneficial for enhancing the mechanical properties of materials. Some of the developed HS metals and alloys exhibited superior mechanical properties, including a strength-ductility synergy [11–29]. Fig. 2(a) summarizes the normalized yield strength (normalized by the corresponding Young's modulus) versus the uniform elongation of HS metals and alloys [13,19–26]. Some data from the homogeneous-structured counterparts of these materials are included for comparison. For conventional metallic materials with homogeneous structures, a strength-ductility trade-off is indicated by the "banana-shaped" curve in Fig. 2(a). In contrast, the corresponding data of HS materials occupying the top-right region lie above the "banana-shaped" curve, indicating that the HS materials can overcome the strength-ductility trade-off. This finding confirms that introducing heterogeneous structures is effective for enhancing strength while maintaining good ductility. This finding also suggests that a desirable strength-ductility synergy can be achieved by regulating the structural heterogeneity, including the volume fraction, morphology, topology and distribution of heterogeneous domains. It is important for the design and fabrication of HS metals and alloys to determine the correlation between the structural heterogeneity and the resultant property enhancement. However, it has been difficult to quantitatively characterize structural heterogeneity, which to some extent restricts the design and fabrication of HS materials. Currently, a few experimental and theoretical studies have been conducted on gradient nanostructured materials, which indicates a relationship between the structural gradient and mechanical properties [19–21].

Currently, most gradient and laminated metallic materials are composed of a CG core sandwiched in between two nanostructured layers. According to the rule of mixtures, a simple way to tailor their mechanical properties is to tune the volume fraction of the CG core (or the nanostructured layers). Recent experimental studies on the GNG steel and multilayered Cu in Fig. 2(a) have shown that the strength values of the gradient samples increase as the thickness of the CG parts decreases; however, this also leads to a certain reduction in uniform elongation [14,15,29]. Moreover, the strength values of the gradient samples can be higher than predictions from the rule of mixture; this discrepancy is mainly ascribed to the long-range internal stress induced by the pile-up and accumulation of GNDs [15]. The contribution of this long-range stress to additional strengthening will be further discussed in the next section. In addition to the volume fractions of the constituents in materials, some microstructural parameters can also be tuned to improve the mechanical properties. As exemplified by the inset in Fig. 2(a), the strength of heterogeneous laminated $Cu/CuZn_{10}$ composites increases with decreasing laminate thickness (i.e., the interface spacing between two adjacent laminates) [21]. Such strength enhancement is attributed to the nucleation and pile-up of higher density GNDs near the interfaces as the laminate thickness decreases [21].

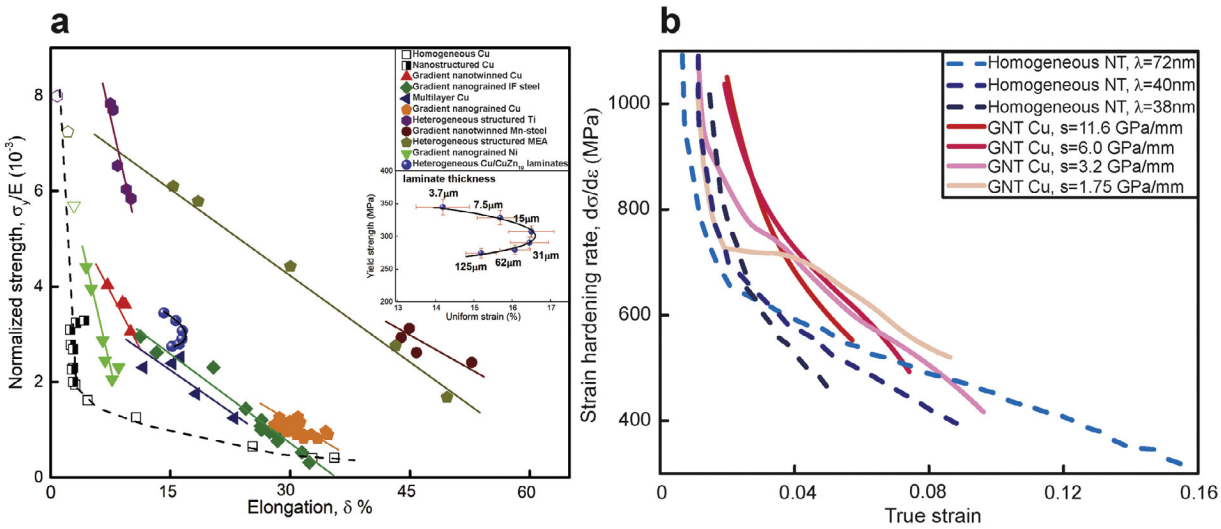

Fig. 2.. Strength-ductility synergy and additional work hardening of some HS metals and alloys. (a) Normalized yield strength (normalized by the corresponding Young's modulus) versus uniform tensile strain of various metals and alloys with homogeneous and heterogeneous structures [13,19–21,26]. (b) Variations in the work hardening rate with respect to the true strain in GNT Cu [20]. (For interpretation of the references to color in this figure legend, the reader is referred to the web version of this article.)

For gradient nanostructured metals, the structural gradient is a key parameter in determining the strength of materials. Recent experimental studies on GNT Cu indicated a relationship between the structural gradient and mechanical properties [20]. The structural gradient distribution of GNT Cu can be controlled by adjusting the processing parameters during direct-current electrodeposition [20]. The structural gradient can be characterized by the gradient variation in local hardness, which is denoted as s. The value of s in the fabricated GNT Cu varies from s=1.75 GPa/mm to s=11.6 GPa/mm. Mechanical testing on these GNT Cu indicated that simultaneous enhancement in strength and work hardening can be achieved by solely increasing the hardness gradient [20]. More interestingly, the tensile strength of the GNT sample with the steepest structural gradient exceeds that of the strongest component of the gradient microstructure [20], indicating additional strengthening. To explain this unusual phenomenon and further elaborate the strain gradient effects on additional strengthening, a gradient plasticity model was recently developed by incorporating the plastic strain gradient into the hardening rate relation of the classical J_2 flow theory [30]. Numerical simulation results showed that the additional strength $\Delta\sigma$ is linearly proportional to the square root of the hardness gradient s (i.e., $\Delta\sigma = \beta\sqrt{s}$, where β is a fitting coefficient) as well as the saturated plastic strain gradient in the fully yielded GNT samples [30]. This nonlinear relationship between the additional strength and structural gradient not only revealed the original additional strength of GNT metals but can also be used to predict the optimal gradient structures and associated gradient strength distributions [30].

In addition to increased strengthening, nearly all HS metals exhibited respectable to superior ductility compared to their CG counterparts [31], as shown in Fig. 2(a). This phenomenon is usually attributed to the additional work hardening capability caused by the heterogeneous structure [14–16,20–26]. Based on Hart's criterion, an increased working hardening rate can ensure stabilized plastic deformation and good ductility. As shown in Fig. 2(b), the work hardening rates of GNT Cu with a dual gradient are much higher than those of gradient-free samples during the overall straining stage [20]. In particular, when the strain is less than 4%, the work hardening rate of GNT Cu increases with increasing structural gradient. This finding indicates that the additional work hardening results from the built-in gradient structure. However, it is noted that as the degree of the gradient becomes stronger, the work hardening rate can decline rapidly due to the disappearance of the plateau stage. Detailed TEM observations showed that the additional work hardening of GNT Cu stems from the formation of bundles of concentrated dislocations (BCDs), which are essentially an assembly or tangle of GNDs [20]. A recent study showed that heterogeneous laminated $CuZn_{10}$ composites exhibited good ductility and a high work hardening rate [21]. The results revealed that the work hardening rate of the laminated $CuZn_{10}$ composites increased with decreasing laminate thickness (i.e., interface spacing). These phenomena are related to the accumulation of GNDs near the interfaces and associated long-range internal stress. Interestingly, there exists a critical laminate thickness corresponding to the maximum elongation, as shown in the inset in Fig. 2(a). In situ high-resolution strain mapping indicated that many GNDs nucleate and then pile up near the interfaces, leading to the formation of an interface-affected zone [21]. When two adjacent interface-affected zones start to overlap, the heterogeneous laminated composite achieves the best ductility. Further theoretical analyses showed that the critical size of the interface-affected zone is half of the laminate thickness and is consistent with the length of the GNDs piling-up against the interface (corresponding to the characteristic length scale of strain gradient plasticity), $l_{GND} \sim (\mu/\sigma_y)^2 b$, where μ is the shear modulus, σ_y is the yield strength and b is the magnitude of the Burgers vector [21].

4. Inhomogeneous deformation and strain gradient plasticity

Owing to the microstructural and strength heterogeneity of different constituent domains, HS metallic materials exhibit inhomogeneous plastic deformation under an applied load. During the deformation of HS materials, plastic yielding progressively propagates from the soft domains to hard domains. Such inhomogeneous deformation has been indicated in a large number of experiments and finite element simulations on the tensile behavior of various HS metallic materials [32–34]. To maintain strain continuity at the continuum level, a pronounced strain gradient is generally generated across the domain interfaces of HS materials. Consequently, many GNDs nucleate and accumulate near the interfaces to accommodate this strain gradient [25]. Fig. 3(a) shows the inhomogeneous deformation process in a dual-phase heterogeneous laminated $AlCoCrFeNi_{2.1}$ high-entropy alloy (HEA), which captures the evolution of the dislocation structures at different deformation

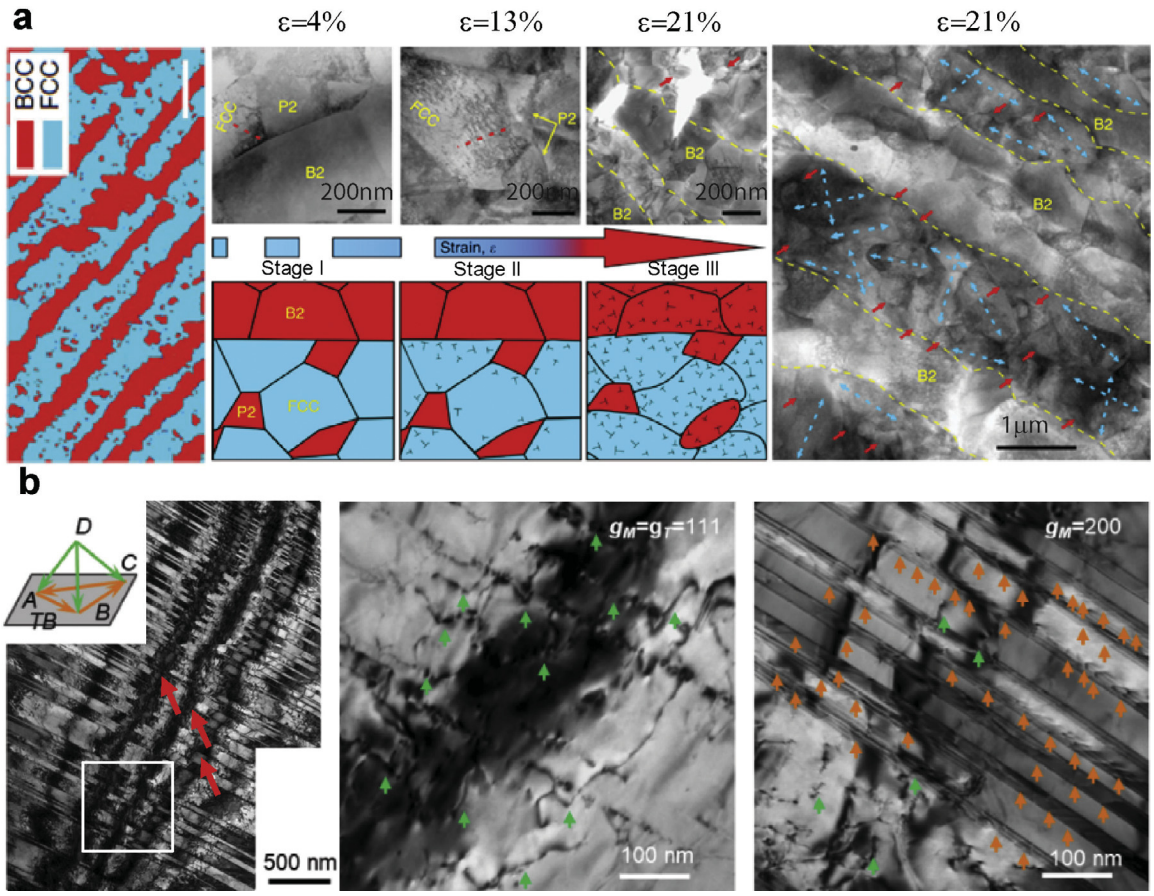

Fig. 3.. Inhomogeneous deformation and evolution of GNDs in some typical HS metals and alloys. (a) Deformation process and microstructural evolution in dual-phase heterogeneous lamella $AlCoCrFeNi_{2.1}$ HEA and corresponding schematic illustrations. This implies the progressive plasticity of soft and hard domains with different phases and the pile-up of GNDs against phase interfaces (indicated by red dashed lines) [35]. (b) TEM images based on the two-beam diffraction technique of the BCD structures in GNT Cu [20]. The BCD indicated by the red arrows is a representative example of the GNDs in GNT Cu. Mode I and II dislocations are indicated by green and orange arrows in (b), respectively. The inset shows the Thompson tetrahedron to identify the Burgers vector of the dislocations. Note that g_M and g_T represent the diffraction vectors of the two beams. (For interpretation of the references to color in this figure legend, the reader is referred to the web version of this article.)

stages [35]. Obviously, the soft face-centered cubic (FCC) matrices first sustain plastic deformation. Due to the constraints from the hard body-centered cubic (BCC) and intergranular P2 phases, a high density of GNDs start to pile up against the interfaces between the soft and hard phases to accommodate the strain gradient, as indicated by the dashed red lines in the TEM image in Fig. 3(a). The pile-up of these GNDs significantly strengthens the heterogeneous HEAs. After both the BCC and P2 phases yield, the FCC matrix will bear more plastic strain to balance the total applied strain, as indicated by the TEM image and schematic illustration in Fig. 3(a). This leads to further strain gradient with ongoing plasticity, which requires more GNDs to accumulate near the interfaces. Fig. 3(b) shows a representative example of GNDs generated during the plastic deformation of GNT Cu with a dual gradient in grain size and twin size [20]. As mentioned in Section 3, in this specific case the GNDs are also called BCDs. Both TEM observations (based on a two-beam diffraction technique) and atomistic simulations showed that a BCD is composed of both mode I and II dislocations, which commonly prevail during plastic deformation of homogeneous NT metals [20]. The mode I dislocations represent dislocations slipping inclined to the twin boundaries, whereas the mode II dislocations represent threading dislocations confined between neighboring twin boundaries. The activities of both types of dislocations lead to strengthening and hardening. The density of mode II dislocations in a BCD is nearly one order of magnitude higher than that of mode I dislocations [20]. The accumulation and interaction of these BCDs not only block further dislocation motion but also facilitate the delocalization of plastic deformation, eventually contributing to high strength and good ductility [20].

Recent experimental studies have shown that the nucleation and accumulation of GNDs significantly contribute to the additional strengthening and hardening of HS metallic materials [14,16,20,35]. The contributions of GNDs to the strengthening of HS materials can be understood in three ways. First, the GNDs can block the motion of other mobile dislocations. Thus, the strengthening effect from GNDs can be described by the Taylor hardening law [8,36,37],

$$\Delta\sigma = M\alpha\mu b\sqrt{\rho_{GND} + \rho_{SSD}} \tag{1}$$

where M is the Taylor factor, α is a material constant (typically 0.2–0.4), μ is the shear modulus of the material, b is the magnitude of the Burgers vector of dislocation, and ρ_{GND} and ρ_{SSD} are the densities of GNDs and SSDs, respectively. Second, when the GNDs pile up against some interfaces or barriers, an internal long-range stress is generated due to the self-stress and interaction of GNDs. This long-range stress, called the back stress, can hinder further dislocation motion. In addition to the forest hardening provided by the GNDs themselves, the back stress is able to contribute to increased strengthening or hardening [16,22,38]. When considering only the self-stress of GNDs with a continuous distribution of density ρ_{GND}, the back stress σ_b is scaled as [39,40]

$$\sigma_b \sim \mu b R^2 \frac{\partial \rho_{GND}}{\partial x} \tag{2}$$

where R is the radius of the integral circular domain for GNDs contributing to the back stress, which is typically on the same order of magnitude as the length of the GND distribution (i.e., a characteristic length scale of strain gradient plasticity [39]), and $\partial\rho_{GND}/\partial x$ represents the first-order derivative of ρ_{GND} with respect to the distribution location. Note that ρ_{GND} is linearly proportional to the strain gradient [2,5,8]. Thus, $\partial\rho_{GND}/\partial x$ represents the second-order derivative of strain with respect to the location, indicating that the back stress is actually related to the second derivative of strain. Third, the nucleation of GNDs accelerates the statistical storage of dislocations during deformation, which is beneficial for additional hardening [37]. According to the Kocks–Mecking–Estrin model, the derivative of the density of SSDs ρ_{SSD} with respect to the plastic strain ε^p can be expressed as [41,42]

$$\frac{\partial\rho_{SSD}}{\partial\varepsilon^p}=M\left(\frac{1}{bL}-k_{ann}\rho_{SSD}\right) \tag{3}$$

where L is the mean free path of dislocations and k_{ann} is the annihilation rate of dislocations, which is related to the strain rate and temperature. The first term in the bracket on the right side of Eq. (3) reflects the dislocation multiplication, whereas the negative second term in the bracket represents the dislocation annihilation due to dislocation reactions or interactions between dislocations and various interfaces. The mean free path of dislocations is a key parameter to describe dislocation interactions and is associated with the grain size d and the total density of dislocations $\rho=\rho_{\mathrm{SSD}}+\rho_{\mathrm{GND}}$. When considering the long-range trapping effect of dislocations, one can obtain an equation for the mean free path of dislocations expressed as $1/L=k_g/d+k_d\sqrt{\rho_{SSD}+\rho_{GND}}$, where k_g is a geometrical parameter related to the grain shape and k_d is a proportionality factor [42]. Eq. (3) has been used in finite element simulations based on the strain gradient plasticity to describe the evolution of SSDs and to investigate their contribution to the deformation of GNG metallic materials [42].

According to previous strain gradient plasticity theory, the density of GNDs is defined as [2,5,8]

$$\rho_{GND}=\frac{1}{b}\frac{\partial\gamma}{\partial x} \tag{4}$$

where γ is the shear strain induced by dislocation slip. Eq. (4) indicates that the density of GNDs is directly linked to the strain gradient. For a polycrystal undergoing uniaxial tension, the density of GNDs within a grain that make up the deformation incompatibility between neighboring grains is approximated as [2]

$$\rho_{GND}\approx\frac{\bar{\varepsilon}}{4bd} \tag{5}$$

where d is the grain size and $\bar{\varepsilon}$ is the applied plastic strain. When modeling HS materials with heterogeneous domains, quantifying the density of GNDs and describing their evolution is a critical issue. In recent models of GNG materials [40,42], the density of GNDs is usually calculated in an average manner. Under plane strain conditions, the GNG sample is modeled as a perfectly bonded multilayered structure with gradient grain sizes from the outermost layer to the core layer. During uniaxial tension, due to plastic instability, the outer layers (with smaller grain sizes) tend to shrink or neck faster in the lateral direction than the inner layers (with larger grain sizes). However, the deformation of the outer layers is constrained by the deformation of the inner layers, leading to nonuniform deformation between adjacent layers. Such deformation can be accommodated by GNDs [40]. In these models, the dislocation line of each GND is assumed to be a straight line along the tensile direction of the sample under plane strain conditions. Thus, the density of GNDs is given by [40]

$$\rho_{GND}=\frac{\zeta}{V}=\frac{a}{b(\Delta h)^2} \tag{6}$$

where ζ represents the total length of GNDs in a unit layer with a thickness of Δh, V is the volume occupied by the GNDs, and a is the displacement difference in the lateral direction between two neighboring layers, which reflects the nonuniform deformation. In recent crystal plasticity simulations for GNG metals [42], the GND density inside a grain is represented by the number of dislocations per unit area, i.e., $\rho_{GND}=N/d^2$, where N is the number of dislocations and d is the grain size. By combining the evolution of the dislocation number N with the plastic strain ε^p, a grain-size dependent evolution law for the GNDs is given by [42]

$$\frac{\partial\rho_{\mathrm{GND}}}{\partial\varepsilon^p}=\frac{N_0}{d^2}\left(1-\frac{N}{N^*}\right) \tag{7}$$

where N_0 represents the initial number of piled-up dislocations and N^* is the saturated number of dislocations. For simplicity, both N_0 and N^* are assumed to be linearly dependent on the grain size [42]. Note that the evolution laws for GNDs and SSDs (Eqs. (3) and (7)) are from theoretical models, but the derivations of these equations involve some empirical or phenomenal assumptions for simplification. The latest experimental studies on heterogeneous copper/bronze laminated composites estimated the density of GNDs via an in situ 2D digital image correlation technique [21,37]. Under uniaxial tension, the average tensile strain ε_y is statistically uniform, whereas the lateral strains ε_x and ε_z of the tested sample exhibit an obvious gradient along the thickness direction x of the sample. Note that to ensure the constant volume of the sample during plastic deformation, $\varepsilon_x+\varepsilon_y+\varepsilon_z=0$. Taking the derivative of this equation, $\varepsilon_x'=-\varepsilon_z'$, where ε_x' and ε_z' are the first-order derivatives of ε_x and ε_z with respect to x, respectively. This equation indicates that due to the structural heterogeneity along the x direction, the gradients in two lateral strains exist only along the x direction and are mutually dependent. According to the original definition (i.e., Eq. (4)) of ρ_{GND} and the deformation features of a heterogeneous laminated sample with two lateral strain gradients, the density of GNDs is re-expressed as [37]

$$\rho_{\mathrm{GND}}=\sqrt{3\varepsilon'_x{}^2+\varepsilon''_x{}^2z^2}/2b \tag{8}$$

where ε_x' and ε_x'' are the first- and second-order derivatives of measured strain ε_x with respect to x, respectively, and z is the z coordinate (i.e., the width direction of the sample). By using the in situ 2D digital image correlation technique to measure the lateral strain ε_x, one can estimate the GND density using Eq. (8) and further characterize the evolution of GNDs in HS metallic materials during plastic deformation.

Fig. 4(a) shows a comparison of the modeling predictions and experimental estimations for the distribution of the GND density along the depth of a GNG sample at different strains. The modeling predictions based on strain gradient plasticity account for the evolution of GNDs and resultant back stress [40]. In contrast, the experimental estimations of the GND density are based on the hardening law due to the generation of GNDs (i.e., Eq. (1)) and experimental measurements of the local hardness distribution of the GNG sample along the depth. Fig. 4(a) shows that the variation trends of the GND density predicted by the model are consistent with those from the experimental estimations. In particular, the maximum values of GND density appear in the gradient layer and near the interface between the gradient layer and the coarse-grained core. Note that there are obvious quantitative discrepancies between the modeling predictions and the experimental estimations. Such discrepancies suggest that the theoretical models cannot accurately capture the evolution of GND density. Fig. 4(b) presents a comparison of the modeling predictions and experimental measurements of the yield strength versus uniform elongation of GNG steels [40]. Fig. 4(b) shows that if the model considers both the GNDs and the back stress, the modeling predictions agree well with the experimental measurements. This find-

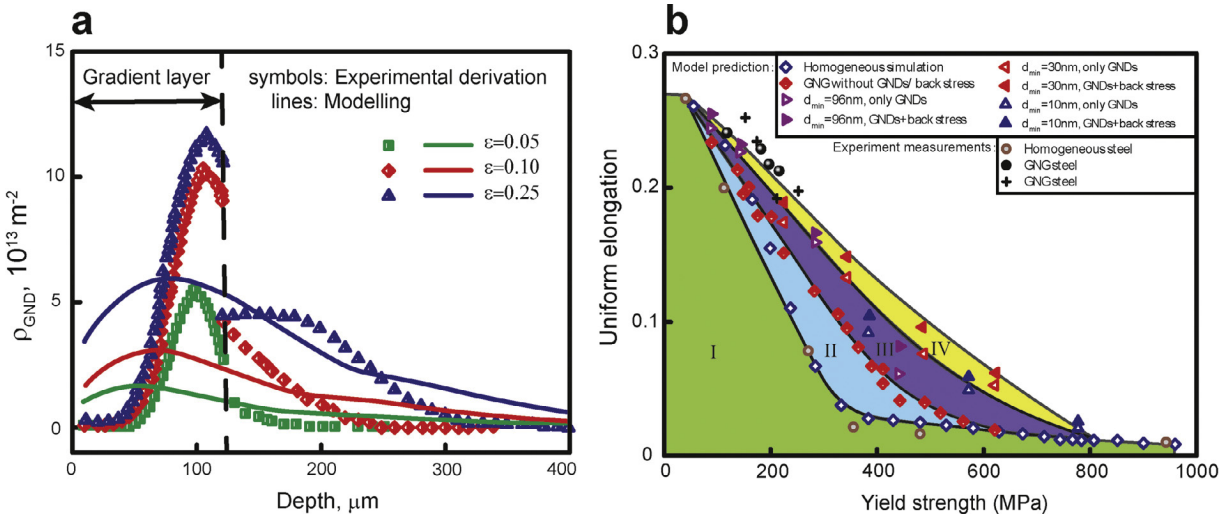

Fig. 4.. Comparisons of the modeling predictions [40] and experimental results for the GND density distribution and the strength-ductility synergy in GNG steels. (a) Comparison of the modeling predictions and experimental estimations for the distribution of the GND density along the depth. (b) Comparison of the modeling predictions and experimental estimations for the yield strength versus uniform elongation. Region I captures the strength-ductility trade-off in homogeneous samples. Regions II, III and IV reflect contributions of the structural gradient, GNDs and back stress to the strength-ductility synergy of GNG samples from the modeling predictions. The symbol "d_{min}" represents the minimum grain size in the gradient layer of the GNG samples. (For interpretation of the references to color in this figure legend, the reader is referred to the web version of this article.)

ing implies that the additional strengthening and work hardening arise from the GNDs including their back stress. Fig. 4(b) quantifies the contributions of the structural gradient, GND and back stress to the strength-ductility synergy of GNG steels from the modeling predictions. Region I reflects the strength-ductility trade-off in homogeneous samples. Region II reflects the contribution from the structural gradient, i.e., without GNDs and back stress. Region III reflects contributions from both structural gradient and GNDs. Region IV reflects contributions from the structural gradient, GNDs and back stress. These findings indicate that the structural gradient and GNDs play a more significant role than the back stress in enhancing the strength and ductility.

As discussed above, the GNDs significantly contribute to additional strengthening and work hardening, especially the synergy between strength and ductility. For HS metallic materials, a quantitative relationship between the structural heterogeneity and GND distribution is essential for a comprehensive understanding of the structure–deformation–property relation of HS materials. It is clear that structural heterogeneity induces the deformation gradient, which further gives rise to the accumulation of GNDs. Therefore, how GNDs evolve with respect to plastic deformation (mainly plastic strain) is an important issue for establishing a relationship between the structural heterogeneity and GND distribution. Currently, there are several theoretical models to describe the evolution of GNDs with respect to plastic strain, but these models are based on certain theoretical assumptions and simplifications, with apparent gaps between the corresponding model predictions and experimental measurements. Therefore, further effort is needed to establish more accurate evolution laws of GNDs in HS metallic materials during plastic deformation, which can be accomplished by combining advanced experimental techniques and theoretical modeling approaches.

5. Perspectives

In summary, experimental, theoretical and computational studies have indicated that introducing structural heterogeneity into engineering metals and alloys is an effective way to achieve strength-ductility synergy and additional work hardening. The inhomogeneous deformation (characterized by a strain gradient) arising from structural heterogeneity gives rise to additional strengthening and hardening of HS metals and alloys. Detailed experimental observations revealed that the nucleation and accumulation of GNDs near the interfaces between soft and hard domains of HS materials play an important role in improving the mechanical properties of these materials. The long-range back stress produced by the interaction of GNDs not only contributes to counteracting the applied stress but also obstructs accumulated dislocations. These results are helpful for elaborating the strengthening and hardening behaviors of HS metals and alloys. However, the relation between the structural heterogeneity and mechanical properties of HS materials is yet to be quantitatively determined. Much of the current design and optimization of HS materials are still based on empirical strategies. Developing more theoretical and computational modeling approaches to quantify the correlation between structural heterogeneity and mechanical properties is necessary for more efficient design and optimization of HS materials. To this end, further effort is needed to develop a unified design principle and mechanistic strategy for HS materials.

To date, most computational models of HS materials have mainly focused on GNS materials. A few mechanism-based models have been recently proposed on the basis of strain gradient plasticity, which were implemented by finite element modeling to study the mechanical properties and behaviors of GNS metals and alloys. These models showed that the enhancement in mechanical properties and behaviors of GNS materials can be quantitatively explained by the strain gradient plasticity involving GND activities and the resultant back stress. A core part of these models is the evolution law of GND density with increasing plastic strain. However, the adopted evolution laws are often hindered by assumptions with various limitations. At this point of time, an open challenge for modeling HS materials is how to establish more accurate, rational and general evolution laws of GND density based on a combination of dislocation dynamics and experimental observations. Once these laws are established, we may be able to investigate more general HS materials with more complicated structures. Furthermore, hierarchical HS materials with multiple characteristic length scales can exhibit greater strengthening and hardening due to the high density of domain interfaces [24,25]. It is interesting to develop both experimental and modeling/simulation techniques for

hierarchical HS materials with multiple length scales. The recent development of digital representation tools may make this possible with the help of EBSD techniques. Integration of better models (involving more accurate evolution laws of GNDs and characterization of structural heterogeneity) and realistic microstructures may open up further opportunities to study the structure–property relationship of HS materials and to guide the design and fabrication of such materials with unprecedented mechanical properties.

Declaration of Competing Interest

The authors declare that they have no known competing financial interests or personal relationships that could have appeared to influence the work reported in this paper.

Acknowledgments

H.G. acknowledges financial support from the National Science Foundation (Grant No. DMR-1709318). X.L. acknowledges financial support from the National Natural Science Foundation of China (Grant Nos. 11522218, 11921002, 11720101002 and 51420105001) and the Beijing Natural Science Foundation (Grant No. Z180014).

References

[1] J.F. Nye, Acta Metall. 1 (1953) 153.
[2] M.F. Ashby, Phil. Mag. 21 (1970) 399.
[3] N.A. Fleck, G.M. Muller, et al., Acta Metall. Mater. 31 (1994) 364.
[4] J.S. Stolken, A.G. Evans, Acta Mater. 46 (1998) 5109.
[5] W.D. Nix, H. Gao, J. Mech. Phys. Solids 35 (1998) 300.
[6] H. Gao, Y. Huang, Scr. Mater. 48 (2003) 113.
[7] N.A. Fleck, J.W. Hutchinson, J. Mech. Phys. Solids 30 (1994) 0714.
[8] H. Gao, Y. Huang, W.D. Nix, et al., J. Mech. Phys. Solids 47 (1999) 1239.
[9] J.L. Bassani, J. Mech. Phys. Solids 2001 (49) (2001) 1983.
[10] Y. Huang, S. Qu, K.C. Hwang, M. Li, H. Gao, Int. J. Plast. 20 (2004) 753.
[11] T. Fang, W. Li, N. Tao, K. Lu, Science 331 (2011) 1587.
[12] K. Lu, Science 345 (2014) 1455.
[13] Y. Wei, Y. Li, L. Zhu, et al., Nat. Commun. 5 (2014) 3580.
[14] X. Wu, P. Jiang, L. Chen, F. Yuan, Y.T. Zhu, Proc. Natl. Acad. Sci. U.S.A. 111 (2014) 7197.
[15] X. Wu, P. Jiang, L. Chen, J. Zhang, F. Yuan, Y.T. Zhu, Mater. Res. Lett. 2 (2014) 185.
[16] X. Wu, M. Yang, F. Yuan, G. Wu, et al., Proc. Natl. Acad. Sci. U.S.A. 112 (2015) 14501.
[17] W. Chen, Z. You, N. Tao, Z Jin, L. Lu, Acta Mater. 125 (2017) 255.
[18] X. Liu, H. Zhang, K. Lu, Acta Mater. 96 (2015) 24.
[19] Y. Lin, J. Pan, H. Zhou, H. Gao, Y. Li, Acta Mater. 153 (2018) 279.
[20] Z. Cheng, H. Zhou, Q. Lu, H. Gao, L. Lu, Science 362 (2018) eaau1925.
[21] C. Huang, Y. Wang, X. Ma, et al., Mater. Today 21 (2018) 713.
[22] X. Wu, Y.T. Zhu, Mater. Res. Lett. 5 (2017) 527.
[23] X. Li, L. Lu, J. Li, X. Zhang, H. Gao, Nat. Rev. Mater. (2020) press.
[24] E. Ma, T. Zhu, Mater. Today 20 (2017) 323.
[25] Y.T. Zhu, X. Wu, Mater. Res. Lett. 7 (2019) 393.
[26] M. Yang, D. Yan, F. Yuan, et al., Proc. Natl. Acad. Sci. U.S.A. 115 (2018) 7224.
[27] C. Sawangrat, S. Kato, D. Orlov, K. Ameyama, J. Mater. Sci. 49 (2014) 6579.
[28] X. Wu, F. Yuan, M. Yang, P. Jiang, C. Zhang, et al., Sci. Rep. 5 (2015) 11728.
[29] X.L. Ma, C.X. Huang, W.Z. Xu, et al., Scr. Mater. 103 (2015) 57.
[30] Y. Zhang, Z. Cheng, L. Lu, T. Zhu, J. Mech. Phys. Solids 140 (2020) 103946.
[31] M.N. Hasan, Y.F. Liu, X.H. An, et al., Int. J. Plast. 123 (2019) 178.
[32] Z. Zeng, X. Li, D. Xu, L. Lu, H. Gao, T. Zhu, Extreme Mech. Lett. 8 (2016) 213.
[33] X. Bian, F. Yuan, X. Wu, Y. Zhu, Metall. Mater. Trans. A 48 (2017) 3951.
[34] Y. Wang, G. Yang, W. Wang, X. Wang, Q. Li, Y. Wei, Sci. Rep. 7 (2017) 10954.
[35] P. Shi, W. Ren, T. Zheng, Z. Ren, et al., Nat. Commun. 10 (2019) 489.
[36] H. Mughrabi, Acta Mater. 54 (2006) 3417.
[37] Y.F. Wang, M.S. Wang, X.T. Fang, et al., Int. J. Plast. 123 (2019) 196.
[38] M. Yang, Y. Pan, F. Yuan, Y.T. Zhu, X. Wu, Mater. Res. Lett. 4 (2016) 145.
[39] C.J. Bayley, W.A.M. Brekelmans, et al., Int. J. Solids Struct. 43 (2006) 7268.
[40] J. Li, G.J. Weng, S.H. Chen, X.L. Wu, Int. J. Plast. 88 (2017) 89.
[41] Y. Estrin, J. Mater. Process. Technol. 80 (1998) 33.
[42] J. Zhao, X. Lu, F. Yuan, Q. Kan, et al., Int. J. Plast. 125 (2020) 314.